An Empirical Line approach for *Agrowing* Camera Aerial Images of inland waters based on exponential fit and *in situ* water measurements

Beatriz Cirino Lucchetta[1], Fernanda Sayuri Yoshino Watanabe[1,2], Nariane Marselhe Ribeiro Bernardo[3], Rafael de Campos Fialho[1], Nilton Nobuhiro Imai[1,2], Antonio Maria Garcia Tommaselli[1,2], Gustavo Soares Roncolato[4]

[1] Graduate Program in Cartographic Sciences, School of Sciences and Technology, São Paulo State University (UNESP), Presidente Prudente, SP 19060-900, Brazil, {beatriz.lucchetta, r.fialho}@unesp.br

[2] Department of Cartography, School of Sciences and Technology, São Paulo State University (UNESP), Presidente Prudente, SP 19060-900, Brazil, {fernanda.watanabe, nilton.imai, a.tommaselli}@unesp.br

[3] Inspectral – Innovative Technology Solutions, Presidente Prudente, SP 19063-390, Brazil, nariane@inspectral.com.br

[4] Graduate Program in Computer Science, School of Sciences and Technology, São Paulo State University (UNESP), Presidente Prudente, SP 19060-900, Brazil, gustavo.roncolato@unesp.br

Keywords: Remote Sensing, Radiometric Calibration, Unmanned Aerial Vehicles (UAV), Multispectral Images, Water Bodies.

Abstract

With the advancement of technology in the area of remote sensing, monitoring the Earth's surface using multispectral cameras attached to unmanned aerial vehicles (UAV) has become promising. However, in many Earth observation applications, it is needed to make compatible the spatial data of images captured by high spatial resolution multispectral sensors with the spectral response of targets on the Earth's surface. This relation is obtained through a radiometric calibration. The empirical line method is commonly used to calibrate the spectral bands of sensors. Thus, applications of this method using linear fit have retrieved negative values in water bodies. So that, attempting different adjustments, as well different reference targets, can solve this issue. In this study, the water quality of small bodies of water was analysed using a *Agrowing* multispectral camera, which derived negative values when applying linear fit. The aim of this study, therefore, was to fit a radiometric calibration based on empirical line method for *Agrowing* camera in inland water applications. Besides of standard reference targets, water samples also were attempted because showed a lower radiance response than the darkest (black) calibration target. Two empirical line methods were applied to convert the digital number (DN) from the *Agrowing* images into remote sensing reflectance (R_{rs}): linear and exponential. The exponential method showed to be more appropriate, with greater accuracy, unlike the linear method.

1. Introduction

The use of unmanned aerial vehicle (UAV) is advantageous in several remote sensing applications, since they allow capturing images of high spatial resolution, providing a high degree of detail for photogrammetric information from the Earth’s surface (Lu and He, 2017). Furthermore, the images do not suffer with atmospheric interference due to the low flight height and is also favourable to different climate and weather conditions, contributing to high temporal resolution of data collection (Wang and Myint, 2015).

When comparing the spatial resolutions of orbital images, commonly used for aquatic monitoring, with images taken from UAVs, it notes that orbital images often make it impossible to monitor small bodies of water, especially due to spatial resolution. On the other hand, images taken from UAVs are suitable for monitoring these targets because of the high spatial resolution. Currently, the use of UAV together with RBG or multispectral sensors (Giles et al., 2022; Dobosz et al., 2023; Wolff et al. 2023; Simes et al., 2024) is on an accelerated rise (Srivastava et al., 2023) for mapping and monitoring of land surface targets, even for monitoring inland water bodies such as lakes and reservoirs (Cao et al., 2023).

According to Cao et al. (2023), different sensors are used to determine limnological variables of water bodies, such as chlorophyll-a, turbidity and suspended material. However, RGB or multispectral cameras store information in digital numbers (DN), which vary with the local lighting condition and sensor consistency (Iqbal et al., 2018). To transform the DN data to true surface reflectance, i.e., to quantify the information obtained by remote sensing, it is necessary to apply a radiometric calibration (Lei et al., 2018).

One of the most used radiometric calibration methods in UAV image is the empirical line, in which is assumed a relationship between the DNs and reflectance values of each channel based on reflectance measurements of calibration targets with different grey levels to promote a certain accuracy of calibration for the data (Wang and Myint, 2015). Commonly, the relationship between DNs and surface reflectances is linear, however, some researchers have found non-linear relationships, depending on the goal and physical principles involved in their work (Staben et al., 2011; Wang and Mying, 2015; Xu et al., 2019; Carmo et al., 2020).

Wang and Mying (2015) found an exponential relationship for calibrating RG-NIR (red, green and near infrared channels) images, using the natural log. Differently, Staben et al. (2011) used a quadratic fit to calibrate images from the Worldview-2 satellite. In turn, Xu et al. (2019) used an empirical line method called Spectral Angle Constraint, which combines the information of spectral reflectance and then adds the spectral information constraint equation.

For remote sensing of water quality, the empirical line method can become challenging, as water bodies have a very low spectral signal, often lower than the darker target (black) adopted for radiometric calibration of images (Pölönen et al., 2014). To solve this problem, Carmo et al. (2020) did not only use an exponential relationship to fit an empirical line, but also samples of water as dark reference target along with conventional calibration panels (white, gray and black).

In this study, two empirical line methods, linear and exponential, were tested for the radiometric calibration of multispectral images captured by the *Agrowing* camera, using calibration panels and samples of the water spectra, with the objective of adapting the best model for radiometric adjustment, since the targets of interest have a low response signal and avoiding negative reflectance. It believes that the exponential fit had shown a better performance, since the attenuation of light in the water column decreases approximately exponentially with depth (Kirk, 2011).

The data acquired with the spectroradiometer in this work showed a water surface reflectance of less than 1% for all targets, making radiometric adjustment difficult. In this paper, partial results of a subsequent estimation of the concentration of chlorophyll-a in small water bodies. It is expected that an adequate radiometric adjustment may contribute to a better discrimination of the optically active components in watercolor remote sensing.

1.1 Objective

This study aimed to fit a radiometric calibration model to aerial images captured by *Agrowing* camera for inland watercolor applications. The specific objectives were: i) to compare linear and exponential fits in calibrating models of radiometric adjustments for inland waters; ii) to investigate the combination of reference standard targets and water measurements collected *in situ* for the adjustment.

2. Methods and Procedures

2.1 Study Area

The study area covers small water bodies located in the National Centre for Research and Conservation of Continental Aquatic Biodiversity (CEPTA) from the Chico Mendes Institute for Biodiversity Conservation (ICMBio), in Pirassununga, São Paulo State (Brazil) (Figure 1).

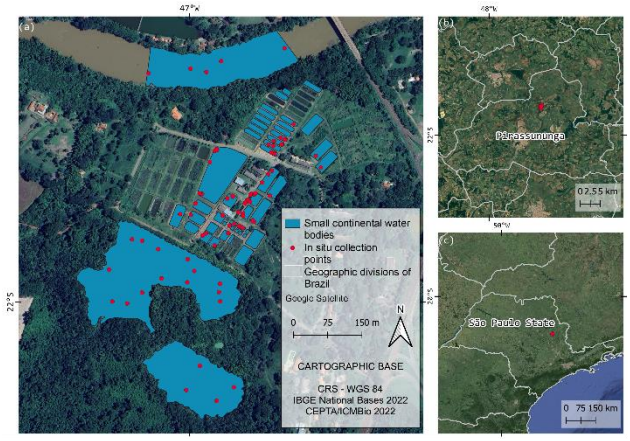

Figure 1. Study area map where (a) the small water bodies are vectorized in blue and the *in situ* collection sampling points are highlighted in red, (b) it show the location in Pirassununga city and (c) the location in São Paulo State.

The site is composed of two reservoirs to feed 128 fish farming tanks, some of which were not analyzed because there is no water, besides a stretch of the Mojiguaçu River, where the tank effluent is released. All water bodies studied have different bio-optical characteristics (Figure 2). The feed reservoirs have a greenish appearance, while the river is brown, with high turbid and large load of suspended sediments. The fish farming tanks also are not like each other. They are built with different structures, some made of concrete and others excavated in the ground, with different fish species that influence the physical chemical parameters of water. Some tanks are darker, others greenish and some have emerged and submerged macrophytes.

The Mojiguaçu River is an anthropically eutrophicated river due to its location near an urban environment. Garbage remains and white foam formations are found there in view of the high pollution. Furthermore, it is a turbid river, with a considerable concentration of suspended material, which turns the water brown. Both tank and feed reservoirs have dense vegetation around them and, therefore, large amounts of organic matter in the water. The appearance is greenish, and although the water is not very turbid, the ground beneath the water is muddy. The concrete fish farming tanks have the smallest extensions of the water bodies analyzed, measuring 1.20 m x 3.50 m. Fixed algae border the tanks, which have a continuous flow of water. On the other hand, macrophytes of different species, flowers and colors emerged from most of the excavated tanks. Some tanks were more greenish and blurred, and others appeared to have dark blue water.

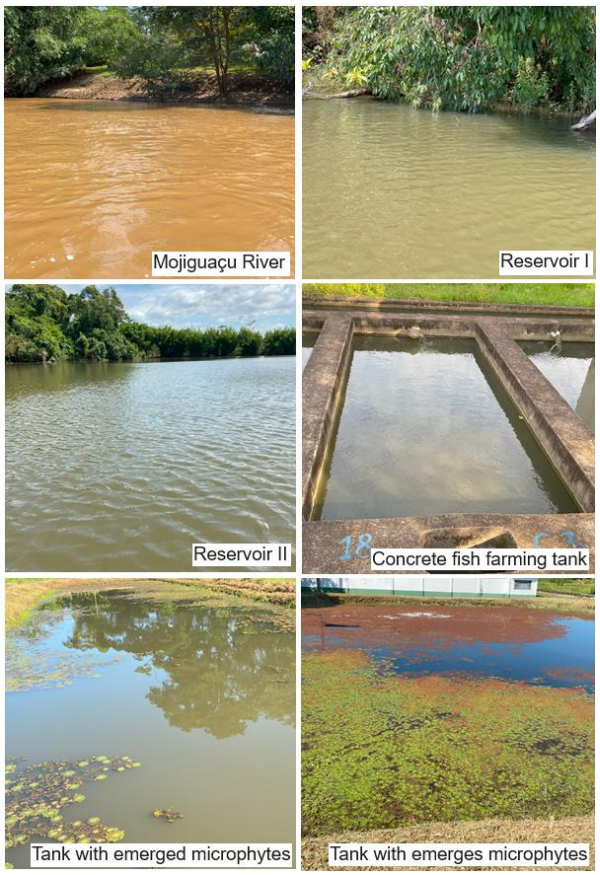

Figure 2. Different water bodies that compound the CEPTA area, with different bio-optical characteristics, including the Mojiguaçu River, the disposal site for water from fish farming tanks; two reservoirs that feed the tanks; and examples of the structure of concrete tanks and excavated tanks with emerged macrophytes.

2.2 Instruments

Three fields’ campaigns were conducted to collect *in situ* radiance measurements, multispectral images and water samples. A *FieldSpec® UV/NIR Handheld* spectroradiometer (ASD, Boulder, CO) (Figure 3) was used to collect *in situ* radiance. The

instrument is capable of capturing light in a spectral range from 350 nm to 1075 nm, with a spectral resolution of 1 nm.

In turn, a *Sony Alpha 7Riv Sextuple* camera (*Agrowing Ltd*.) was used to acquire multispectral images. This camera has six heads (Figure 4) and 14 narrow spectral bands. Figure 5 shows the transmittance spectrum of each band from *Agrowing* camera. Technical specifications of camera are presented in Table 1. Table 2 shows the central wavelength of each band and the full width half maximum (FWHM).

The camera was attached to an UAV *Matrice 300 RTK* (DJI Innovations) (Figure 6). The *Matrice 300 RTK* platform has four propellers, take-off weight maximum of 9 kg, power battery of 5935 mAh and an estimated flight time of 20 minutes, approximately. According to their manufacturer, the UAV has a design for professional aerial photography (DJI Innovations).

Figure 3. *FieldSpec® UV/NIR Handheld* spectroradiometer measuring a highly diffuse reflectance calibration plate in a laboratory, with the aid of a halogen light.

Figure 4. *Sony Alpha 7Riv Sextuple* camera (*Agrowing* camera), with six heads.

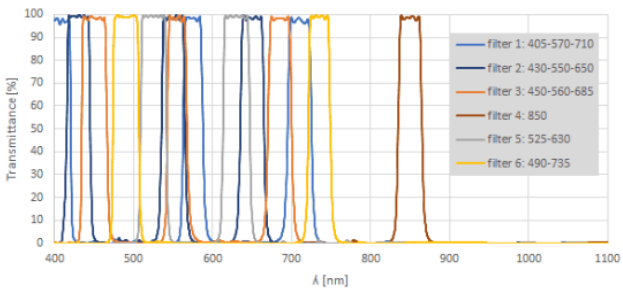

Figure 5. Transmittance of camera *Agrowing* filters (Adapted from https://agrowing.com/products/alpha-7riv-sextuple/).

Characteristics	Parameters
Type	Sextuple lens single mount
Field of view	Diagonal: 45.9º; Horizontal: 35º; Vertical: 26.6º
Lens distortion	<1%
Relative illumination	68%
Focal length	21.26 mm
Focus type and range	Manual 2.5mm to infinity
Lens size	60 mm x 35.2 mm
Lens weight	180 g
Total weight with battery	845 g
Flight height	120 m

Table 1. *Sony Alpha 7Riv Sextuple* camera characteristics, provided by *Agrowing Ltd.*

Bands	Central wavelength (nm)	Bandwidth (mm)
1	405	25
2	430	25
3	450	25
4	490	25
5	525	25
6	550	25
7	560	25
8	570	25
9	630	25
10	650	25
11	685	25
12	710	10
13	735	10
14	850	15

Table 2. Central wavelength and bandwidth of the 14 bands of *Agrowing* camera.

Figure 6. *Matrice 300 RTK* platform (UAV).

2.3 Data Acquisition

Three field campaigns were carried out on February 16th and 17th, 2022; February 14th, 15th, and 16th, 2023; and July 21st, 2023. A total of 69 samples were collected in different water bodies, as shown in Figure 1. Radiometric measurements were collected using a *ASD FieldSpec® handheld* spectroradiometer, following the protocol proposed by Mueller (2003) for water.

Firstly, dark current reading is done and then, the spectroradiometer is optimized using a highly diffuse reflectance plate. The reference plate radiance (L_g) spectrum was taken, followed by the total radiance (L_t), which corresponds to the

leaving-water radiance (L_w) plus the radiance reflected by the water surface (L_r). Both L_g and L_t were measured with the sensor pointed at 45° in relation to nadir. In turn, the incident radiance from the sky (L_s) was measured, with the sensor pointed at 45° in relation to the zenith.

In addition, the sensor is always oriented orthogonally in relation to the solar azimuthal plane. The radiance measurements acquired *in situ* were used to calculate the remote sensing reflectance (R_{rs}), using Mobley (1999) (Equation 1).

$$R_{rs} = \frac{L_t - \rho L_s}{\frac{\pi}{R_g} L_g} \quad (1)$$

To make the spectroradiometer's measurements compatible with the images captured by *Agrowing* camera, a band simulation was applied using R_{rs} spectrum. This procedure is performed through spectral convolution operation, multiplying spectral data by the spectral filter function (S_B), integrating the result for wavelengths in the channel and normalizing by the band width (Burggraaff, 2020), as shown in Equation 2.

$$\bar{R}_{rs}^{B} = \frac{\int_{\lambda \epsilon B} L_w(\lambda)\, S_B(\lambda)\, d\lambda}{\int_{\lambda \epsilon B} E_d(\lambda)\, S_B(\lambda)\, d\lambda} \quad (2)$$

where $L_w(\lambda)$ = water-leaving radiance

$E_d(\lambda)$ = downward irradiance

$S_B(\lambda)$ = spectral response function of each instrument band

$\int_{\lambda \epsilon B} d\lambda$ = wavelength in the band

$S_B(\lambda)$ from *Agrowing* camera is not available, hence it was approximated to a Gaussian function. The images used in this study were captured on July 21st, 2023, between 10 a.m. and 2 p.m. Before the flight, with the aid of the spectroradiometer, the radiances of the calibration (reference) targets were measured in the field, in the same lighting conditions as the images were taken. The radiance values also were used to determine R_{rs} and the band simulation was also applied to these data.

Reference plates (0.5 m x 0.5 m) made of ethyl, vinyl and acetate (E.V.A) were used as calibration targets, in four different colors: white, light gray, medium gray and black. E.V.A plates were also placed in the field to be captured by camera and used to calibrate the images radiometrically.

The *Agrowing* camera has its own calibration plate, indicated by the manufacturer, with 24 colors produced with barium sulfate (Figure 7). Experiments were carried out with this plate, however, good results were not obtained from the radiometric calibration, limiting the use only of the available E.V.A. panels. It is noteworthy that the white target of the E.V.A. panel was not used for the empirical line, due to the overestimation of the brightness of the target. One of the reasons for not using the colorimetric plate was that grayscale targets resulted in a higher brightness when compared to the white target. Other colors also were not used because it noted that the red color had a shift of its spectral curve to the near-infrared wavelengths.

Figure 7. Colorimetric plate with 24 colors which has been tested for radiometric calibration of images.

To cover the entire area, two flights of approximately 20 minutes were carried out, with a flight height of 90 m and exposure time of 1/800 s. The day was sunny, without cloud cover and with a light breeze, which did not interfere the flight plan.

2.4 Images Processing

The raw images taken by the *Agrowing* camera were geometrically processed before applying the empirical line method. To process the images, firstly, *Agrowing Basic* software, in the demo version, was used to identify and align the 14 spectral bands, in addition to transforming data in the .RAW extension to the .TIFF extension in DN, 8 bits. From the .TIFF images, it was possible to stack the image bands and build an orthomosaic of the study area, using the *Agisoft Metashape* software. The initial Ground Sampling Distance (GSD) of the images was 1.17 cm, which will later be resampled to a GSD of 10 cm, to facilitate subsequent processing. The DN values of the resultant images were used to develop the empirical line.

2.5 Radiometric Calibration for Empirical Line

Radiometric measurements from calibration plates taken *in situ* were used to calibrate the images, converting the DN of the pixels into R_{rs} values, using the empirical line technique. It is worth mentioning that the images radiometric resolution is 8 bits (DN – 0 to 255). The empirical line was applied individually to each of the 13 *Agrowing* camera bands used in this study. The band with an wavelength centered at 405 nm was not applied, as it is in the ultraviolet region of the electromagnetic spectrum, which is not important for this work. Two functions were used to convert DN into R_{rs}, exponential and linear, described by Equations 3 and 4.

$$Rrs = a \times e^{b(DN)} \quad (3)$$

$$Rrs = a \times (DN) + b \quad (4)$$

It is worth mentioning that besides the calibration standard targets, a water sample, with the lowest value of R_{rs}, was added to compose the calibration model. This sample was used because the darkest reference target has a greater R_{rs} than the water targets. Experiments showed that using only E.V.A plates results in negative values of R_{rs}.

2.6 Accuracy Assessment

The performance of radiometric calibration models was evaluated using coefficient of determination (R^2), normalized root means square error (NRMSE) and bias, using 54 points out of the total of 68, once detected outliers were excluded, expressed by Equations 5, 6 and 7, respectively.

$$R^2 = 1 - \frac{\sum(x_i - x_{est,i})^2}{\sum(x_i - x_{meas,i})^2} \quad (5)$$

$$NRMSE = \left(\frac{\sqrt{\frac{1}{n}\sum_i^n (x_{est,i} - x_{meas,i})^2}}{x_{max} - x_{min}} \right) \times 100 \quad (6)$$

$$bias = \frac{1}{n}\sum_{i=1}^{n} x_{est,i} - x_i \quad (7)$$

where x = variable
$x_{meas,i}$ = measured values of i^{th} reflectance data
$x_{est,i}$ = estimated values of i^{th} reflectance data
x_{max} = maximum value of reflectance data
x_{min} = minimum value of reflectance data

3. Results and Discussions

Despite the high precision of the radiometric calibration performed in several studies of water bodies with the use of images from orbital and aircraft sensors, the *Agrowing* camera is a new instrument, whose processing flow was defined for water targets, exclusively, for this work. The *Agrowing* camera, according to the manufacturer, was developed and is excellent for mapping and monitoring vegetation. The sensor was tested for water due to bands of interest for the mapping of limnological parameters and the possibility of obtaining high spatial resolution images. Bands with the central wavelength at 650 nm and 685 nm, close to the maximum absorption in the red region, are related to the chlorophyll-a component, as well bands centered at 710 nm and 735 nm associated with suspended sediments and chlorophyll-a.

Figure 8 shows R_{rs} spectrum simulated by *Agrowing* bands for some sampling points. Among them, the sample P68 was used to develop the empirical line models for each spectral band. This sample was selected because it has the lowest R_{rs} values of the water collected on the day the image capture flight was made.

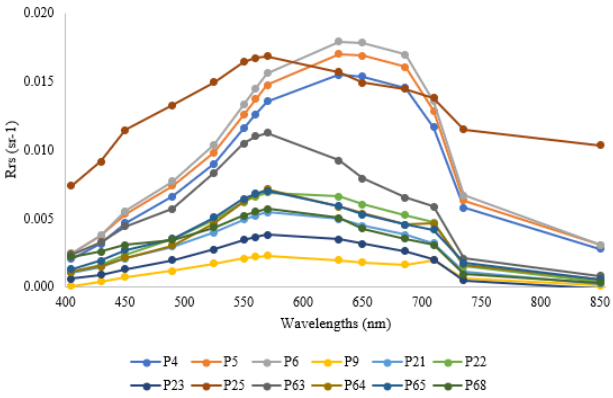

Figure 8. Reflectance spectral curves of some sample points, including P68, which was used to develop the empirical line models.

3.1 Calibration Equations

Figure 9 shows the fitted models for spectral bands centered at 570 nm (green), 630 nm (red), 710 nm (red-edge) and 735 nm (red-edge), employing exponential (left column) and linear (right column) empirical line models.

These bands were chosen to presentation because they are important channels for the development of bio-optical models in inland waters. It is noted that the linear empirical models for bands at 710 nm and 735 nm estimate negative R_{rs} values. This likely happens because the calibration targets, including the water sampling point, have “high” reflectance values compared to other radiometric responses from collected sampling points. Therefore, exponential fits were tested to solve the problem of negative value prediction. It is known that R_{rs} ranges from 0 to 1, so that, negative values are erroneous.

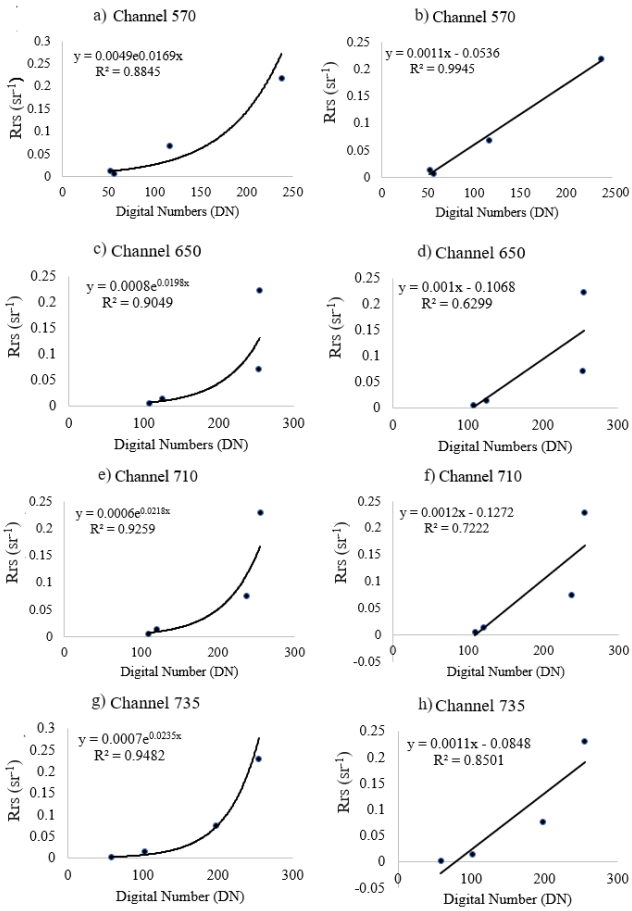

Figure 9. Exponential and linear empirical line graphs in left column (a, c, e and g) and right column (b, d, f and h), respectively.

Figure 10 shows part of the water bodies (rivers and some tanks) in the study area. Fig. 10a displays a true-color composition (RGB-650, 550 and 450 with the pixels in DN values, 8 bits). Fig. 10b shows the same are in R_{rs} values after applying the linear model, while Fig. 10c presents R_{rs} values, resulting the exponential model. Fig. 10d was taken from Google Earth. Visually, it notes that the resultant images have different colors. When the results of the reflectance (Fig. 10b and Fig. 10c) are compared with the true color image from Google Earth (Fig. 10d), it is noted that the colors of the water bodies between the result of the exponential calibration (Fig. 10c) and the Google Earth (Fig. 10d) image are closer, whereas the resulting image of the linear calibration model showed grayish and bluish colorations for the water bodies.

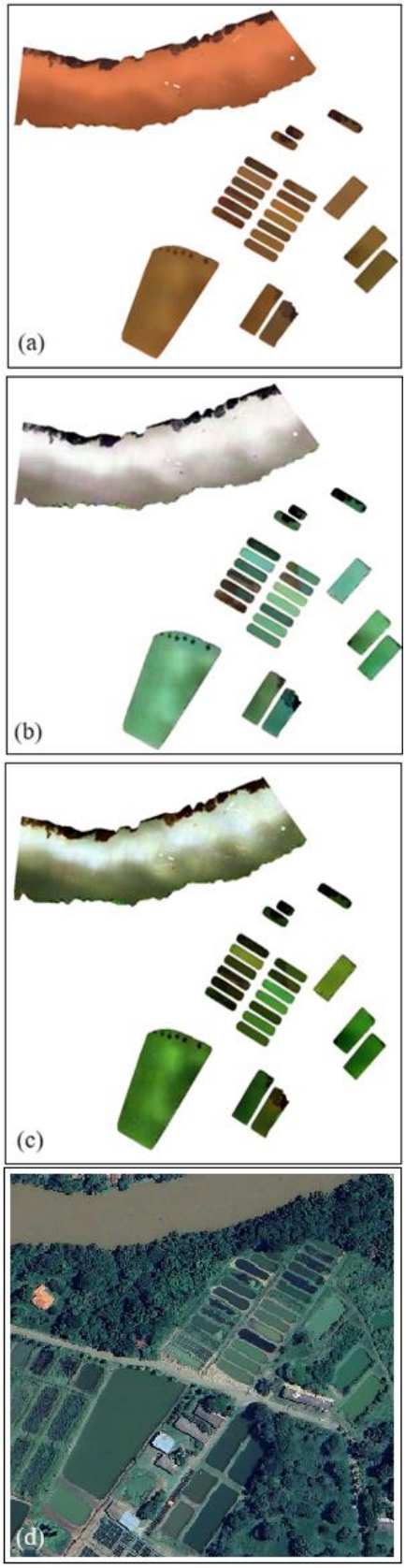

Figure 10. Part of the study area, where (a) is the matrix image in DN values, (b) is the matrix image with the application of linear empirical model, reflectance values, (c) is the matrix image with the application of exponential empirical model, reflectance values and (d) is an image from Google Earth.

3.2 Validation Results

Table 3 presents the results of the model evaluation, considering R^2, NRMSE and bias errors. Analyzing the bands separately, only bands centered at 630, 650, 685 and 710 nm did not reach an R^2 above 0.80 for the linear model, while for the exponential model the R^2 is above 0.81 for all channels. Regarding NRMSE, the linear models exhibited very high errors for all bands, with values above 100%. In contrast, the exponential models presented errors greater than 100% only for bands 630 nm and 650 nm.

Radiometric adjustment for water targets has been a challenge for many researchers, since water highly absorbs solar radiation and calibration targets end up being “brighter” than *in situ* targets, making it difficult to achieve a good adjustment (Gao et al., 2010). In this work, the white and light gray calibration targets reached maximum DN values in the images captured for the red-edge and visible-red bands, preventing the model from being well adjusted for these channels.

The inaccuracy of the models observed by the bias values is greater for bands at 630 nm and 650 nm for the exponential adjustment, and almost for all bands of the linear adjustment, except for the bands in the visible green region.

Bands	R^2		NRMSE (%)		bias	
	Exponential	Linear	Exponential	Linear	Exponential	Linear
430	0.87	0.97	48.14	228.19	0.002	-0.007
450	0.91	0.96	49.04	186.80	0.002	-0.001
490	0.90	0.97	62.76	160.73	0.004	0.001
525	0.91	0.97	66.85	154.95	0.006	0.009
550	0.91	0.97	65.01	188.53	0.007	0.021
560	0.93	0.97	61.15	166.61	0.008	0.020
570	0.88	0.99	58.95	138.07	0.008	0.017
630	0.91	0.64	211.09	298.97	0.018	0.031
650	0.91	0.63	118.92	258.88	0.010	0.026
685	0.96	0.78	85.07	231.62	0.007	0.016
710	0.93	0.72	92.25	321.14	0.007	0.027
735	0.95	0.85	31.99	238.08	0.001	-0.007
850	0.81	0.97	50.82	404.09	0.001	-0.011

Table 3. R2, NRMSE and bias of the calibration models, exponential and linear, applied to images from the Agrowing camera.

For future work, images displayed in this study will serve as a basis for the development and application of bio-optical models for estimating chlorophyll-a concentration. So that, the red-edge and visible-red bands are essential to predict pigment concentration (e.g., Gitelson et al. 2008; Gurlin et al. 2011; Mishra and Mishra, 2012). Therefore, it will be necessary to adopt strategies to minimize the high errors achieved through radiometric calibration. However, the exponential model was promising in calibrating images captured by the *Agrowing* sensor for water targets.

In addition, since the targets have a low signal response, calculating the camera's signal-to-noise ratio can help improve and understand the results. Another alternative may be to test higher flight heights to avoid specular reflection. Increasing the GSD also can help to obtain a greater amount of energy within a pixel.

4. Conclusions

This study used a methodological approach based on empirical line method for the radiometric calibration of images from the *Agrowing* multispectral camera, coupled to the UAV, which captured images of small inland water bodies. The linear fit found in the literature, using at least two calibration targets (white and black), has good performance in mapping terrestrial targets.

However, the results of this study showed a better performance for an exponential fit in inland waters. In addition, the use of traditional calibration targets along with *in situ* R_{rs} values of water samples also supported to improve the calibrated model performance. The outcomes observed in this study, therefore, contribute to improving the performance of radiometric calibration for high spatial resolution images in inland water application, and for mapping and monitoring aquatic systems and environments.

Acknowledgements

The authors would like to thank Inspectral Startup for all the support and instruments provided; São Paulo Research Foundation – FAPESP for the Thematic Project (Process N. 2021/06029-7), and the PIPE 2 Project (Process N. 2021/11296-4); also, Coordenação de Aperfeiçoamento de Pessoal de Nível Superior - CAPES (88887.310313/2018-00) and National Council for Scientific and Technological Development - CNPq (303670/2018-5), for funding and research grants. Acknowledgements to School of Science and Technology from São Paulo State University UNESP and the Post-graduate Program on Cartographic Sciences (PPGCC). They would also like to thank National Centre for Research and Conservation of Continental Aquatic Biodiversity (CEPTA) from the Chico Mendes Institute for Biodiversity Conservation (ICMBio), for providing support and access to field sites during the development of this study.

References

Bemis, S. P., Micklethwaite, S., Turner, D., James, M. r., Akciz, S., Thiele, S. T., Bangash, H. A., 2014: Ground-based and UAV-Based photogrammetry: A multi-scale, high-resolution mapping tool for structural geology and paleoseismology. *Journal of Structural Geology* 69, 163 – 178. doi.org/10.1016/j.jsg.2014.10.007

Burggraaff, O., 2020: Biases from incorrect reflectance concolution. *Optics Express* 28(9), 13801-13816. doi.org/10.1364/OE.391470

Cao, Q., Yu, G. & Qiao, Z., 2023: Application and recent progress of inland water monitoring using remote sensing techniques. *Environmental Monitoring Assessment* 195, 125. doi.org/10.1007/s10661-022-10690-9

Carmo, A. F. C., Bernardo, N. M. R., Imai, N. N., Shimabukuro, M. H., 2020: Improving the empirical line method applied to hyperspectral inland water images by combining reference targets and *in situ* water measurements. *Remote Sensing Letters* 11(2), 186 – 194. doi.org/10.1080/2150704X.2019.1692383

Dobosz, B., Gozdowski, D., Koronczok, J., Žukovskis, J., Wójcik-Gront, E., 2023: Evaluation of Maize Crop Damage Using UAV-Based RGB and Multispectral Imagery. *Agriculture* 13, 1627. doi.org/10.3390/agriculture13081627

Gao, H., Gu, X., Yu, T., Gong, H., Li, J. G., Li, X. Y., 2010: HJ-1A HSI on-orbit radiometric calibration and validation research. Science China Technological Sciences 53, 3119–3128. doi.org/10.1007/s11431-010-4113-2

Giles, A. B., Correa, R. E., Santos, I. R., Kelaher, B., 2024: Using multispectral drones to predict water quality in a subtropical estuary. *Environmental Technology* 45(7), 1300–1312. doi.org/10.1080/09593330.2022.2143284

Gitelson, A. A., Dall’olmo, G., Moses, W., Rundquist, D. C., Barrow, T., Fisher, T. R., Gurlin, D., Holz, J., 2008: A simple semi-analytical model for remote estimation of chlorophyll-a in turbid waters. *Remote Sensing of Environment* 12, 3582 – 3593. doi.org/10.1016/j.rse.2008.04.015

Gurlin, D., Gitelson, A. A., Moses, W. J., 2011: Remote estimation of Chl-a concentration in turbid productive waters-Return to a simple twoband NIR-red model? *Remote Sensing of Environment* 115, 3479–3490. doi.org/10.1016/j.rse.2011.08.011

Iqbal, F., Lucieer, A., Barry, K., 2018: Simplified radiometric calibration for UAS-mounted multispectral sensor. *European Journal of Remote Sensing* 51, 301–313. doi.org/10.1080/22797254.2018.1432293

Kirk, J. T. O., 2011: *Light & Photosynthesis in Aquatic Ecosystems*. London: Cambridge University Press, 3th Ed, 665.

Lei, D., Hao, X., Mao, Z., Yan, Y., Jie, S., Zhang, A. A., 2018: Subband Radiometric Calibration Method for UAV-Based Multispectral Remote Sensing. *IEEE Journal of Selected Topics in Applied Earth Observations of Remote Sensing* 11, 2869–2880.doi.org/ 10.1109/JSTARS.2018.2842466

Lu, B., He, Y., 2017: Species classification using Unmanned Aerial Vehicle (UAV)-acquired high spatial resolution imagery in a heterogeneous grassland. *ISPRS Journal of Photogrammetry and Remote Sensing* 128, 73 – 85. doi.org/10.1016/j.isprsjprs.2017.03.011

Mishra, S., Mishra, D. R., 2012: Normalized difference chlorophyll index: A novel model for remote estimation of chlorophyll-a concentration in turbid productive waters. *Remote Sensing of Environment* 117, 394 – 406. doi.org/10.1016/j.rse.2011.10.016

Mobley, C. D., 1999: Estimation of the remote-sensing reflectance from above-surface measurements. *Applied Optics* 38, 7442-7455. doi.org/10.1364/AO.38.007442

Mueller, J. L., 2003: In-water radiometric profile measurements and data analysis protocols. In: Ocean Optics Protocols for Satellite Ocean Color Sensor Validation, Revision 4, Volume III: Radiometric Measurements and Data Analysis Protocols. Mueller, J. L.; Fargion, G. S.; McClain, C. R. (Eds.). NASA Goddard Space Flight Space Center: Greenbelt, MD, EUA, 7-20.

Pölönen, I., Puupponen, H.H., Honkavaara, E., Lindfors, A., Saari, H., Markelin, L., Hakala, T., Nurminen K., 2014: UAV-based hyperspectral monitoring of small freshwater area. *Remote Sensing for Agriculture, Ecosystems, and Hydrology XVI*, 923912. doi.org/10.1117/12.2067422

Simes, T., Pádua, L., Moutinho, A., 2024: Wildfire Burnt Area Severity Classification from UAV-Based RGB and Multispectral Imagery. *Remote Sensing* 16(1), 30. doi.org/10.3390/rs16010030

Srivastava, A., Prakash, J. Techniques, 2023: Answers, and Real-World UAV Implementations for Precision Farming. *Wireless Personal Communications* 131, 2715–2746. doi.org/10.1007/s11277-023-10577-z

Staben, G. W., Pfitzner, K., Bartolo, R., Lucieer, A., 2012: Empirical line calibration of WorldView-2 satellite imagery to

reflectance data: using quadratic prediction equations. *Remote Sensing Letters* 3(6), 521–530. doi.org/10.1080/01431161.2011.609187

Wang, C.; Myint, S. W., 2015: A Simplified Empirical Line Method of Radiometric Calibration for Small Unmanned Aircraft Systems-Based Remote Sensing. *IEEE Journal of Selected Topics in Applied Earth Observations and Remote Sensing* 8(5), 1876 – 1886. doi.org/ 10.1109/JSTARS.2015.2422716

Wolff, F., Kolari, T H. M., Villoslada, M., Tahvanainen, T., Korpelainen, P., Zamboni, P. A. P., Kumpula, T., 2023: RGB vs. Multispectral imagery: Mapping aapa mire plant communities with UAVs. *Ecological Indicators* 148, 14. doi.org/10.1016/j.ecolind.2023.110140.

Xu, K., Gong, Y., Fang, S., Wang, K., Lin, Z., Wang, F., 2019: Radiometric Calibration of UAV Remote Sensing Image with Spectral Angle Constraint. *Remote Sensing* 11(11), 1291. doi.org/10.3390/rs11111291